Appl. Sci. Converg. Technol. 26(4): 74-78 (2017)
http://dx.doi.org/10.5757/ASCT.2017.26.4.74

Research Paper

Investigation of the Driving Frequency Effect on the RF-Driven Atmospheric Pressure Micro Dielectric Barrier Discharges

Hyowon Bae[a], Jung Yeol Lee[b], and Hae June Lee[b]
[a]*Memory Division, Samsung Electronics, Hwaseong, South Korea*
[b]*Department of Electrical and Computer Engineering, Pusan National University, Busan 609-735, South Korea.*

Received June 26, 2017; revised July 29, 2017; accepted July 30, 2017

Abstract The discharge characteristics of the radio frequency (RF) surface dielectric barrier discharge have been simulated for the investigation of the ratio of the ion transit time to the RF period. From one-dimensional particle-in-cell (PIC) simulation for a planar dielectric barrier discharge (DBD), it was observed that the high-frequency driving voltage confines the ions in the plasma because of a shorter RF period than the ion transit time. For two-dimensional surface dielectric barrier discharges, a fluid simulation is performed to investigate the characteristics of RF discharges from 1 MHz to 40 MHz. The ratio of the peak density to the average density decreases with the increasing frequency, and the spatiotemporal discharge patterns change abruptly with the change in the ratio of ion transit time to the RF period.

Keywords: Dielectric barrier discharge, Atmospheric pressure plasma, The effect of driving frequency

I. Introduction

Atmospheric pressure plasmas (APPs) attracts lots of attentions for its easy applications without the necessity of an expensive vacuum system [1]. The dielectric barrier discharge (DBD) is the most common method to sustain plasmas with a voltage of a few kilovolts and frequencies of tens of kilohertz [2]. Stable glow discharges are generated at atmospheric pressure with the help of the dielectric barrier, which lowers the substation voltage by the additional wall voltage by the accumulated charged during the previous half cycle of a time-varying applied voltage. That is to say, after a half cycle of the sinusoidal driving voltage ends, the sustain voltage for the next half cycle decreases because the previously accumulated charges enhance the voltage difference during the opposite phase of the applied voltage. Another advantage of the DBD is that the dielectrics prevent the transition of the discharge mode from a glow to an arc because the accumulated wall charges always decrease the effective voltage between the electrodes. Therefore, a stable low-temperature plasma can be generated within the DBD devices.

It is also possible to add gas flow within the structure of two facing electrodes, which is called a plasma jet. It is necessary to shorten the tube size to make a long plasma flume with a plasma jet, but it results in the small interaction area. The dielectric barrier discharges with facial electrodes also have a limitation for the gap distance because of Paschen's law because the breakdown voltage increases as the gap distance increases. Therefore, the concept of a microplasma array [3] or a planar micro-discharge cell [4] is a good way to generate a large area plasma source. However, the elaborate patterning is required for the microplasma array, which sometimes costs a lot. Thus, the surface DBD with patterned electrodes is a better way to extend the microplasmas to a large area [5, 6]. The surface DBD is also very effective to generate plasmas in the air without He or Ar gas flow. For example, the ambient gas plasma is utilized for ozone generation or disinfection of surfaces [6].

In this study, we investigate the effect of the driving frequency on the discharge characteristics using a one-dimensional particle-in-cell (PIC) simulation and a two-dimensional fluid simulation. In Sec. II, we present the simulation conditions followed by the simulation results shown In Sec. III. Finally, summary and conclusion are presented in Sec. IV.

II. Simulation Conditions

The one-dimensional PIC simulation is based on the conventional PIC method utilizing a leap-frog scheme for the particle mover and linear weighting for the particles to grids and fields to the particles [7,8]. For the collision with background neutral gas, the Monte Carlo collision (MCC) scheme is installed in the simulation code using the null-

*Corresponding author
E-mail: haejune@pusan.ac.kr

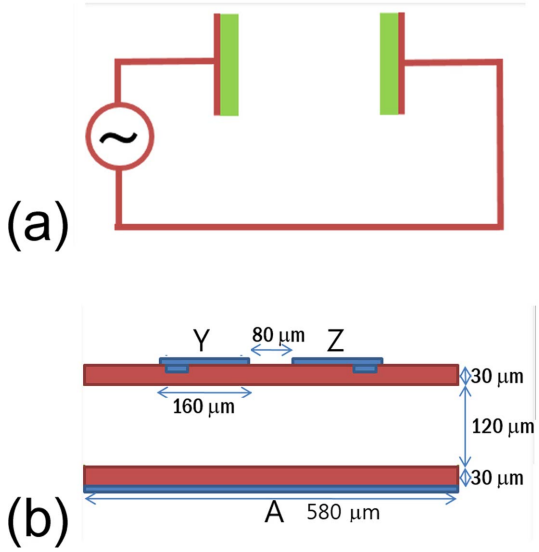

Figure 1. (a) A schematic model of dielectric barrier discharge is shown. The red parts consist of a power source that drives voltage through the gas-filled gap between two parallel conducting electrodes. The green bars are the dielectric barriers on each electrode (b) Two-dimensional simulation structure for the considered planar UV light source. The red blocks are dielectric materials and the gas-filled gap. The blue blocks are electrodes. Upper electrodes are the Y (right) and Z (left) electrode. The lower electrode The A is electrode.

collision method [9]. Elastic scattering, excitation, and ionization collisions are considered for the electron-neutral collisions. For ion-neutral collisions, charge exchange and scattering are considered. Figure 1(a) shows the structure of one-dimensional planar DBD with a gap distance of 80 mm for pure Ar discharge. The thickness of the dielectric barrier is set to be 10 mm on each electrode. The relative permittivity is 5. A sinusoidal external voltage is applied to the left-hand side electrode. Also, the secondary electron emission coefficient (SEEC) is set to 0.1 for argon ions bombarding on the dielectric surface. We did not consider the dependency of SEEC on the energy and angle of the incident ions for simplicity. However, in general, a higher energy and a large incident angle result in a larger SEEC. The simulation time step is on the order of 2 fs, and the grid size is smaller than 0.5 mm to calibrate the size of electron Debye length.

The simulation condition for a two-dimensional planar discharge is the same as our previous paper for the coplanar micro DBDs [10,11] with Xe and Ne gas mixture. It solves the governing equations of the Poisson's equation and the continuity equations of ions and electrons. The considered gas mixture includes charged species of electrons, Xe^+, Ne^+, Xe_2^+, Ne_2^+, and $NeXe^+$. The considered excited species are $Xe^*(^3P_1)$, $Xe^*(^3P_2)$, $Xe_2^*(O_\mu^+)$, $Xe_2^*(^1\Sigma_\mu^+)$, $Xe_2^*(^3\Sigma_\mu^+)$, Xe**, and Ne*. The considered gas pressure is set to 400 Torr, and the drift-diffusion approximation is appropriate for the estimation of the fluxes of charged particles. Also, for this high pressure, all of the transport coefficients such as diffusion coefficient and mobility as well as reaction coefficients for ionizations and excitations are calculated as a function of E/p, where E is the electric field intensity, and p is the gas pressure. For this simulation case, the gas mixture ratio of Ne:Xe is set to 8:2. The geometric shape is shown in Fig. 1(b). Here, the electrodes Y and Z have a sinusoidal driving voltage of $0.5V_0\sin\ \omega t$ and $-0.5V_0\sin\ \omega t$ respectively, and the electrode A is grounded. The relative permittivity of the top and the bottom dielectrics are 17 and 7, repectively. In the pracital applications of open surface DBDs, the electrode A and the dielectric on it are not necessary. However, it is effective to have the grounded booundary in a simulation so that Poisson's equation can reach a unique solution much faster. However, the simulation results with open space show the same tendency, and thus the existence of the grounded electrode A does not change the physics at all. This will be explained in Sec. 3 again with Fig. 7.

III. Results

Figure 2 shows the result of the measured firing voltages over the variation of the driving frequency observed by the one-dimensional PIC simulation mentioned in Sec. II. When the applied voltage is larger than the firing voltage, a gas breakdown happens. The firing voltage shows two different tendencies. At first, if the driving frequency is less than 10 MHz, the firing voltage is increasing with the increase of the driving frequency in a scaling law of $f^{0.55}$, where f is the driving frequency. However, the firing voltage decreases with the increase of the driving frequency in a scaling law of f^{-1} when the driving frequency is larger than 10 MHz. This drastic change of the firing voltage is caused by the heating mode transition. At high frequency, the a-process is dominant in electron generation while the g-process is dominant at a lower frequency. The physics of this transition was explained in our previous research for He DBD discharges [12], and the same physics happens even in Ar discharge which has

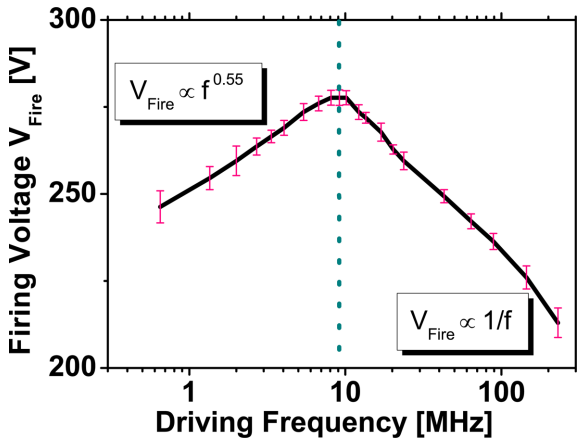

Figure 2. the amplitude of firing voltage with driving frequency dependency in the 80-μm gap is shown as log-log scale plot. This plot indicates two breakdown voltage scaling laws with input frequency.

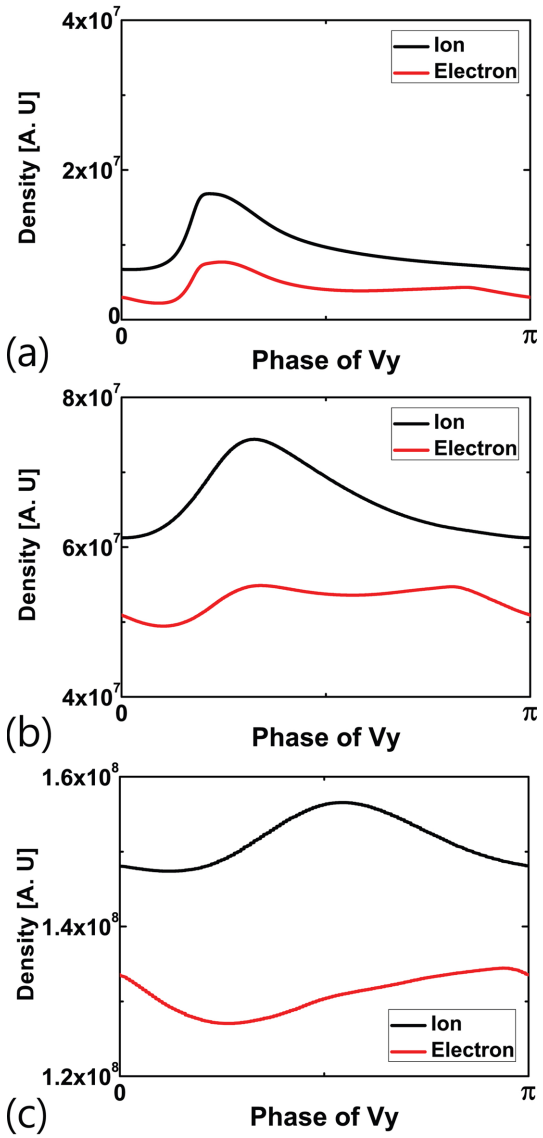

Figure 3. The two-dimensional discharge model is used to show the time-averaged density of electric charge in the gap. The x-axis is time phase of (a) 1, (b) 10, and (c) 40 MHz sinusoidal waveform of voltage on Y electrode.

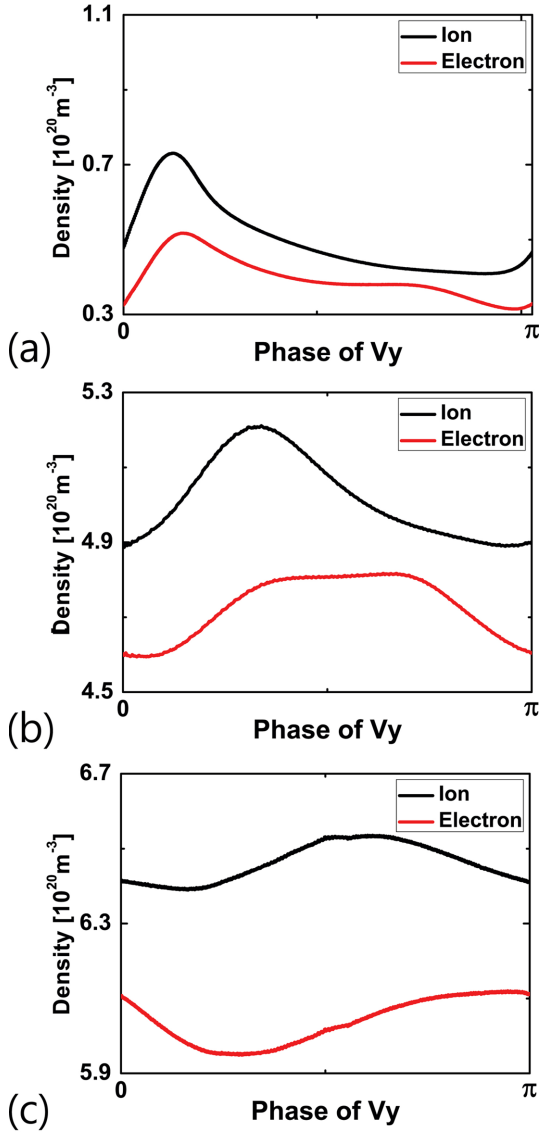

Figure 4. The one-dimensional PIC model is used to show the time-averaged density of electric charge in the gap. The x-axis is time phase of (a) 5, (b) 40.68, and (c) 162.72 MHz sinusoidal waveform of voltage on Y electrode.

Ramsauer mininum in its elastic collision cross-section. Another important physics is that the scaling law for the low frequency and the high frequency regime are the same for He and Ar discharges although the energy relaxation mean free path (λ_ε) for the He discharge is less than the gap distance while λ_ε of Ar discharge (about 250 μm) is larger than the gap distance. It was also observed in the previous research that the one-dimensional DBD has maxinum ionization efficiency when the ratio of ion transit time to the RF period is about 1/4 [12]. That is to say, the secondary electrons emitted by ion bombardment on the cathode are accelerated effectively during the acceleration phase in the sheath if the ion transit time is about a quarter of the RF period.

In this study, our main interest is to investigate the effect of ion transit time on the surface DBD system. In a two-dimensional surface DBD, the electric field profiles are two-dimensional, and thus the ion transit time is affected by the geometry also. Figure 3 shows the temporal evolution of electron and ion densities for a half RF cycle for the variation of the driving frequency, 1 MHz, 10 MHz, and 40 MHz. The peak voltage difference between the Y and Z electrode, V_0, is fixed to 290 V. The ion density is the total sum of all positive ions in the system. Because of the symmetry in the geometry, the density results are periodic during a half RF cycle. The peak density at the steady state increases with the driving frequency, which are $1.75 \cdot 10^7$, $7.45 \cdot 10^7$, and $1.57 \cdot 10^8$ for ions and $8.12 \cdot 10^6$, $5.47 \cdot 10^7$, and $1.34 \cdot 10^8$ for electrons with a driving frequency of 1 MHz, 10 MHz, and 40 MHz, respectively. This increase is caused by the decreasing wall loss with the increase of the driving frequency rather than the increase of the ionization. The wall loss is mainly caused by the ion transport, which can be controlled by the ratio of the ion

transit time to the RF period. Also, it is noticeable that the difference between the peak density to the average density decreases with the increasing driving frequency. The ratio of the maximum to the minimum ion densities during a half cycle is 2.51, 1.21, and 1.0621 for the driving frequency of 1 MHz, 10 MHz, and 40 MHz, respectively. Another important feature of Fig. Three is that the time evolutions of the electron and the ion densities show dephasing oscillation in 40 MHz case, which is caused by the ion inertia which cannot follow the time-varying field promptly at a high frequency.

We also tested similar cases with a one-dimensional PIC simulation, which are shown in Fig. 4. With the increasing frequencies of 5 MHz, 40.68 MHz, and 162.72 MHz, the same tendency is shown for the increasing peak plasma densities and the decreasing peak to average density ratio. In Fig. 2, the case with a frequency of 5 MHz is located at a left-hand side of the peak breakdown voltage, which is different from those with 40.68 MHz and 162.72 MHz which are located on the right-hand side of Fig. 2. The case for the two-dimensional simulation has a longer system size with a heavy Xe species, and thus the mode transition happens at a lower frequency than that of the one-dimensional system.

For the case with a driving frequency of 1 MHz, Fig. 5 shows the spatial evolution of the density profiles of electrons and the excited state, Xe*($^3P_1$), during a half cycle at a different phase of the driving voltage. With a driving frequency of 1 MHz, the ion transit time is shorter than the driving RF period. Therefore, the plasma density decreases rapidly by the ambipolar diffusion when the driving voltage is not large enough to induce ionization. At the initial phase, the remaining electron density is small and localized as shown in Fig. 5(a). When the applied

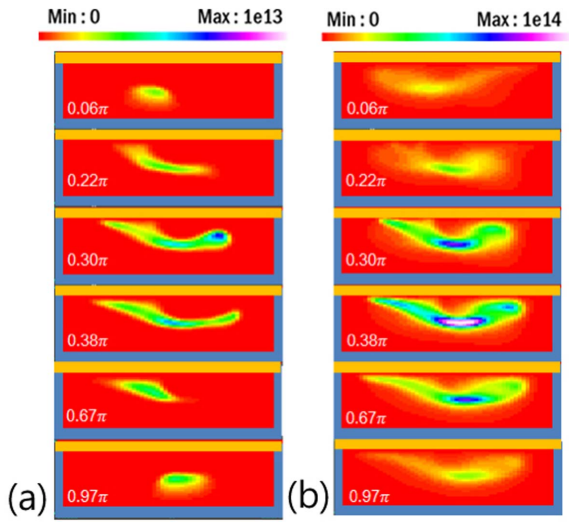

Figure 5. By 1 MHz of applied voltage waveform, Spatio-temporal evolutions of the density of electrons on left side hand and the radiative excited state, Xe*($^3P_1$) on right side hand, are shown for the phase difference from the rising time of applied voltage waveform on Y electrode.

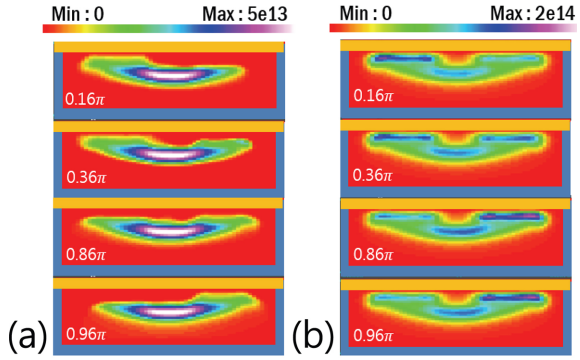

Figure 6. By 10 MHz of applied voltage waveform, Spatio-temporal evolutions of the density of electrons on left side hand and the radiative excited state, Xe*($^3P_1$) on right side hand, are shown for the phase difference from the rising time of applied voltage waveform on Y electrode.

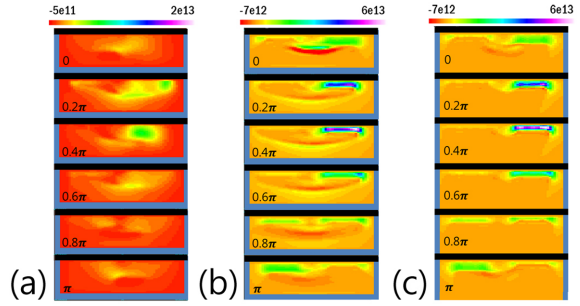

Figure 7. Spatio-temporal evolutions of the density net charge, are shown for the phase difference from the rising time of applied voltage waveform on Y electrode. Figure (a) and (b) show evolutions for 120 μm-sized gap discharge induced by 1 MHz and 10 MHz of applied voltage waveform from Y electrode. Figure (c) show evolutions for the upper part of 450 μm-sized gap discharge induced by 10 MHz of applied voltage waveform from Y electrode.

voltage increases as time go on, the electron density increases again because of active ionization. The excited state density of Xe* has a peak value near 1/4 phase as shown in Fig. 5(b). However, both the electron and the Xe*($^3P_1$) densities decrease again when the applied voltage decreases because of ion transport.

Figure 6 shows the spatial evolution of the density profiles of electrons and the excited state, Xe*($^3P_1$), during a half cycle for the case with a driving frequency of 10 MHz. In this case, the ion transit time is longer than the RF period. That is to say, the external fields are reversed before ions escape the system, which decreases the ion transport abruptly. Therefore, the electron density profiles have the almost constant shape at the center except for the cathode sheath as shown in Fig. 6(a). Meanwhile, the Xe*($^3P_1$) density shows maximum values near the electrodes and at the center as shown in Fig. 6(b). The excitation happens a lot near the sheath because the electrons get enough energy at the sheath, and also at the center because the electron density is large there.

Figure 7 shows the comparison of the case with a bottom electrode as shown in Fig. 1(b) with the ground an

electrode at the bottom. The comparison of fig. 7(b) and (c) shows that extended gap helps to remove net charge accumulation in middle position, not plasma sheath region near induced electrodes. However, most of the tendency is the same because the role of the electrode is mainly to minimize the simulation time.

IV. Conclusions

From a one-dimensional particle-in-cell (PIC) simulation for a planar dielectric barrier discharge (DBD), it was observed that the breakdown voltage decreases with the increasing driving frequency because the high-frequency driving voltage confines the ions in the plasma due to a shorter RF period than the ion transit time. For two-dimensional surface dielectric barrier discharges, a fluid simulation is also performed to investigate the characteristics of RF discharges with an increasing driving frequency. The plasma density increases with the increasing driving voltage mainly because the wall loss of ions decreases. The ratio of the peak density to the average density decreases with the increasing frequency, and the spatiotemporal discharge patterns change abruptly with the change in the ratio of ion transit time to the RF period.

Acknowledgments

This work was supported by Basic Science Research Program through the National Research Foundation of Korea funded by the Ministry of Education, Science and Technology (Grant No. 2016M3A9C6918285).

References

[1] H. W. Lee, G. Y. Park, Y. S. Seo, Y. H. Im, S. B. Shim, and H. J. Lee, J. Phys. D: Appl. Phys. 44, 053001 (2011).
[2] B. Eliasson, M. Hirth, and U. Kogelschatz, J. Phys. D: Appl. Phys. 20, 1421 (1987).
[3] J. G. Eden and S. J. Park, Plasma Phys. Control. Fusion 47, B83 (2005).
[4] D. S. Lee, K. Tachibana, H. J. Yoon, and H. J. Lee, Jpn. J. Appl. Phys. 48, 056003 (2009).
[5] J. Pons, E. Moreau, and G. Touchard, J. Phys. D: Appl. Phys. 38, 3635 (2005).
[6] M. J. Pavlovich, H.-W. Chang, Y. Sakiyama, D. S. Clark, and D. B. Graves, J. Phys. D: Appl. Phys. 46, 145202 (2013).
[7] C. K. Birdsall and A. B. Langdon, Plasma Physics via Computer Simulations (Adam Hilger, Bristol, 1991).
[8] J. P. Verboncoeur, Plasma Phys. Controlled Fusion 47, A231 (2005).
[9] V. Vahedi and M. Surendra, Comput. Phys. Commun. 87, 179 (1995).
[10] H. W. Bae, H.-J. Lee, and H. J. Lee, Appl. Sci. Converg. Technol. 25, 6 (2016).
[11] S. B. Shim, I. C. Song, H.-J. Lee, and H. J. Lee, J. Appl. Phys. 110, 023301 (2011). \
[12] J. Y. Lee, H. W. Bae, H. J. Lee, and J. P. Verboncoeur, Plasma Sources Sci. Technol. 23, 035017 (2014).